Evolution of the Electron Distribution Function in the Presence of Inverse Bremsstrahlung Heating and Collisional Ionization

A. L. Milder, H. P. Le, M. Sherlock, P. Franke, J. Katz, S. T. Ivancic, J. L. Shaw, J. P. Palastro,
A. M. Hansen, I. A. Begishev, W. Rozmus, and D. H. Froula

Evolution of the electron distribution function in the presence of inverse bremsstrahlung heating and collisional ionization

A. L. Milder,[1,2] H. P. Le,[3] M. Sherlock,[3] P. Franke,[1,2] J. Katz,[1] S. T. Ivancic,[1] J. L. Shaw,[1] J. P. Palastro,[1] A. M. Hansen,[1,2] I. A. Begishev,[1] W. Rozmus,[4] and D. H. Froula[1,2]

[1]*Laboratory for Laser Energetics, 250 E. River Rd, Rochester, NY 14623, USA*
[2]*Department of Physics and Astronomy, University of Rochester, Rochester, NY 14623, USA*
[3]*Lawrence Livermore National Laboratory, 7000 East Avenue, Livermore, CA 94550, USA*
[4]*Department of Physics, University of Alberta, Edmonton, Alberta T6G 2E1, Canada*
(Dated: October 30, 2019)

The picosecond evolution of non-Maxwellian electron distribution functions was measured in a laser-produced plasma using collective electron plasma wave Thomson scattering. During the laser heating, the distribution was measured to be approximately super-Gaussian due to inverse bremsstrahlung heating. After the heating laser turned off, collisional ionization caused further modification to the distribution function while increasing electron density and decreasing temperature. Electron distribution functions were determined using Vlasov-Fokker-Planck simulations including atomic kinetics.

Electron velocity distributions govern fundamental processes in plasma physics. Models of these processes often take the electron distribution function to be Maxwellian or include a small perturbation about a Maxwellian. While this assumption can lead to significant errors, any deviation from a Maxwellian requires a kinetic understanding, which is often prohibitively challenging. However, as computational resources improve and experiments begin to isolate kinetic effects, an understanding of non-Maxwellian electron distribution functions is becoming more tractable.

In laser-produced plasmas, inverse bremsstrahlung heating [1–3], thermal transport [4, 5], laser-plasma instabilities [6], and atomic kinetic processes [7] all provide competing mechanisms that govern the shape of the electron distribution function. A recent computational study has shown the impact of atomic kinetics on inverse bremsstrahlung heating and nonlocal thermal transport, through modifications of the electron distribution function [7]. In a separate study, non-Maxwellian electron distribution functions driven by thermal transport were shown to modify Landau damping of electron plasma waves and enhance their corresponding instabilities [5]. Furthermore, most atomic physics models used to calculate x-ray emission for plasma characterization are built assuming a Maxwellian electron distribution and deviation from a Maxwellian modifies these calculations [2].

Although there have been numerous computational studies of kinetic effects in hydrodynamics over the last forty years [8], experiments have been challenged to isolate changes to the electron distribution function. In the 1990s, microwaves were used in low-temperature ($\sim$ 1 eV), low-density ($< 10^{17}$ cm^{-3}) plasmas to investigate changes to the electron distribution function introduced by inverse bremsstrahlung heating [9]. Later in the decade, initial studies in laser plasmas suggested the existence of non-Maxwellian electron distribution functions using Thomson scattering [10]. More recently, Thomson-scattering experiments were able to show the effect of nonlocal thermal transport on electron distribution function [4].

In this Letter, we present the first measurements of the interplay between inverse bremsstrahlung heating and ionization kinetics on the electron distribution function. An ultrafast Thomson-scattering system was used to collect the electron plasma wave spectrum, which enabled the picosecond evolution of the non-Maxwellian electron distribution function to be measured in a laser-produced plasma. The preferential heating of the slow electrons by a laser beam with an intensity of 2.5×10^{14} W/cm^2, coupled with the redistribution of electron kinetic energy due to ionization, resulted in a non-Maxwellian electron distribution function. The shape of the electron distribution function, 60 ps into the plasma formation, was measured to be approximately a super-Gaussian of order 3.4. After the laser turned off, the electron density continued to increase by 15% over the next 40 ps ($\sim$ 25 electron-ion collision times) due to collisional ionization. Over this time, the electron temperature decreased from 400 eV to 300 eV, which is consistent with the energy required for collisional ionization to increase the density. To determine the electron distribution functions consistent with the measured Thomson-scattered spectra in this rapidly evolving plasma, Vlasov-Fokker-Planck simulations that included laser heating, thermal transport and ionization were required. Laser heating was found to have the largest effect on the shape of the distribution function, while atomic kinetics provided a smaller effect, it was required to match the evolution of plasma conditions.

Thomson-scattering experiments were performed using the Multi-Terawatt laser [11] at the Laboratory for Laser Energetics. Figure 1 shows the experimental configuration where a 1.053 µm, $P = 0.08$ TW, 60 ps square pulse laser beam was focused $\sim$1.4 mm before the center of a gas jet using an $f/9$ geometry. The diameter
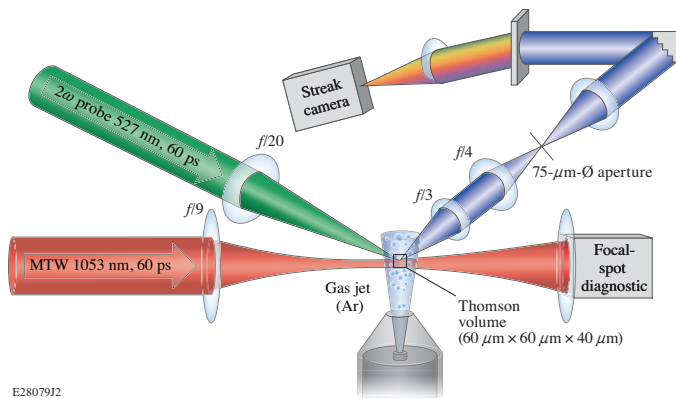
FIG. 1. A schematic of the experiment is shown with the heater (red) and probe (green) beams incident on the gas jet. The heater beam was imaged on a focal-spot diagnostic. Thomson-scattered light was collected by an $f/3$ optic at 80° relative to the probe beam (resulting in a 100° scattering angle).

of the approximately Gaussian focal spot at the center of the gas jet was measured in vacuum to be 200 µm ($r = 100$ µm) [Full width at half maximum (FWHM)], which provided a spatially ($A = \pi r^2$) averaged intensity of $I = P/A = 2.5 \times 10^{14}$ W/cm^2. A supersonic Mach 3 gas jet [12] with an exit diameter of 1 mm was pressurized with argon (Ar) to 50 psi to achieve a neutral gas density of 2.4×10^{18} cm^{-3} at 1 mm above the nozzle. A 527 nm, linearly chirped (0.05 nm/ps), 60 ps square pulse Thomson-scattering probe beam, with a spatially averaged intensity of $\sim 10^{14}$ W/cm^2, was focused at $f/20$, 1 mm above the nozzle, to the center of the gas jet with an angle of 43° to the heater beam. The Thomson-scattering probe beam arrived at the interaction volume 40 ps after the heater beam, resulting in a 20 ps temporal overlap of the beams.

The Thomson-scattered light from a 60 µm × 60 µm × 40 µm volume at the center of the gas jet was passed through a 532 nm dielectric notch filter with a spectral width of 28 nm to reject the portion of the spectrum associated with ion acoustic waves, or other scattering of the probe beam. The collimated light was imaged to the 75 µm input aperture of an ultrafast streaked spectrometer system [13] by an $f/4$ achromat. The $f/3$ pulse-front-tilt compensated spectrometer was coupled to an ultrafast optical streak camera (ROSS P820).

The spectrometer used an echelon to trade unrealized resolving power for improved temporal resolution. The temporal response function was measured with a fully compressed pulse from the Multi-Terawatt laser system to be 2.2 ps FWHM [14]. The spectral instrument response (1.27 nm FWHM) and the spectral dispersion were measured using the emission lines of a mercury lamp. The spectral instrument response was dominated by the diameter of the entrance aperture of the spectrom-
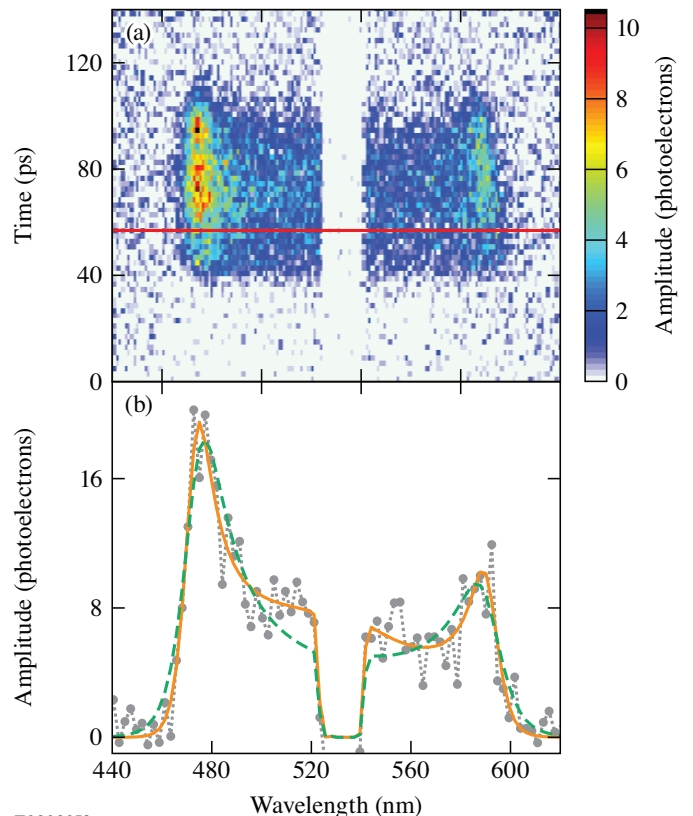
FIG. 2. (a) Thomson-scattering spectrum measured from a plasma heated by an intensity of 2.5×10^{14} W/cm^2. The heater beam begins at t=0 ps and the probe beam at t=40 ps. (b) The measured spectrum at 58 ps (gray points) plotted with spectrum calculated using Maxwellian (dashed green curve) and non-Maxwellian (orange curve) electron distribution functions. The best-fit spectra determined T_e= 423 eV, n_e= 2.03×10^{19} cm^{-3}, m= 2 (Maxwellian) and T_e= 406 eV, n_e= 2.04×10^{19} cm^{-3}, m= 3.1 (Non-Maxwellian).

eter. The measured spectra were corrected for group delay dispersion from the optics, spectral throughput, and sweep curvature introduced by the streak camera.

Figure 2 shows a Thomson-scattering spectrum measured from an argon plasma. The angle between the Thomson-scattering probe beam and the collection optics (80°) was chosen to maximize the ability to determine the shape of the electron distribution function. The electron plasma wave spectral features were clearly resolved along with the light scattered between the features, which results from the relatively large Landau damping ($k\lambda_D \sim 0.6$, where λ_D is the Debye length). The spectra throughout have been summed over two resolution units in wavelength and time.

The spectrum [Fig. 2(b)] just prior to turning off the heater beam (~ 58 ps) shows the effect of inverse bremsstrahlung heating through the modification of the electron distribution function and the need to include non-Maxwellian electron distribution functions to accu-
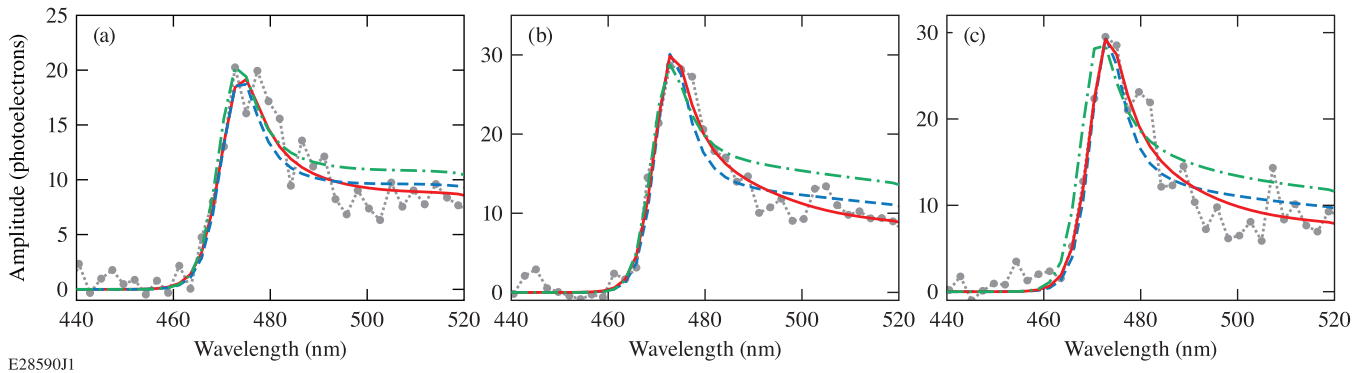
FIG. 3. Measured (grey points) Thomson-scattering spectra at (a) 58 ps, (b) 71 ps, and (c) 78 ps are shown with the results from K2 simulations with (red curve) and without (dashed blue curve) the atomic physics model, which best represent the data. The results from K2 simulations without the atomic physics model, but adjusted to have the same temperature as the simulation with atomic physics is shown as the dash-dotted green curve.

E28590J1

rately reproduce the measured spectra. When limiting the spectral fit to Maxwellian electron distribution functions, the spectrum fails to reproduce three regions of the measurements: (1) the calculations underestimate the light scattered into the central region of the spectrum ($\sim$500 nm to $\sim$550 nm), (2) the widths of the scattering features are too broad, and (3) the slope on the outermost edges of the scattering peaks are too shallow.

When calculating the spectra in Fig. 2, a super-Gaussian electron distribution function was assumed, $f_m = C_m \exp[-(v/v_m)^m]$, where $v_m^2 = \frac{3k_B T_e}{m_e} \frac{\Gamma(3/m)}{\Gamma(5/m)}$ and C_m is a normalization factor [2]. This super-Gaussian shape is a result of slow electrons being preferentially heated by inverse bremsstrahlung, causing a depletion of the slow electrons and an addition of thermal electrons [1]. The super-Gaussian order (m) was predicted to be dependent on the relative strength of inverse bremsstrahlung and electron-electron collisions [2]. The given functional form for the electron distribution preserves the standard definitions of temperature (T_e) and density (n_e) in relation to the velocity moments. A super-Gaussian electron distribution function significantly improves the fit in all three of the regions discussed earlier and reduces the χ^2 per degree of freedom from 3.75 to 1.33. This large improvement in χ^2 per degree of freedom is a result of the model doing a better job matching the center of the variation, instead of the edge, removing any systematic trends from the residuals.

The calculated spectra were determined through a 3-dimensional (m, T_e, n_e) $\chi^2 = \sum_\lambda \frac{[P(\lambda) - P_s(\lambda)]^2}{1.15 P_s(\lambda)}$ minimization of the measured spectrum $[P_s(\lambda)]$ and the calculated power [15], which is approximately

$$P(\lambda) \propto \left(1 + \frac{2\omega}{\omega_0}\right) \left[\frac{1}{k}\left|\frac{1}{1+\chi_e}\right|^2 f_e\left(\frac{\omega}{k}\right)\right] \frac{d\omega}{d\lambda}, \quad (1)$$

where the wave vector ($\mathbf{k} = \mathbf{k}_0 - \mathbf{k}_s$) and frequency ($\omega = \omega_0 - \omega_s$) of the probed fluctuations are given by the

Thomson-scattering probe laser ($\omega_0, \mathbf{k}_0$) and the resulting scattered light ($\omega_s, \mathbf{k}_s$). The electron susceptibility,

$$\chi_e(\mathbf{k}, \omega) = \int_{-\infty}^{\infty} d\mathbf{v} \frac{4\pi e^2}{m_e k^2} \frac{\mathbf{k} \cdot \partial f_e/\partial \mathbf{v}}{\omega - \mathbf{k} \cdot \mathbf{v}}, \quad (2)$$

was determined numerically. Here, m_e and e are the electron's mass and charge, respectively. The calculated scattered power was adjusted to account for the finite aperture effects in the data [16] and the spectral response of the instrument.

Figure 3 shows the evolution of the Thomson-scattering spectrum after the heating laser was turned off. Due to the rapidly evolving conditions, the Thomson-scattering spectra were calculated using electron distribution functions from the Vlasov-Fokker-Planck code K2 [17], which is 1 dimensional in space and 3 dimensional in velocity (1D3V). When including both inverse bremsstrahlung heating and thermal conduction in the simulations, the calculated Thomson-scattering spectra are in reasonable agreement with the measured features (Fig. 3 dashed blue curve). K2 includes elastic collision operators for electron-electron collisions in addition to terms describing inverse bremsstrahlung heating and thermal transport, including self-consistent electric fields and return currents [17].

Figure 4 shows that it is necessary to include ionization in the K2 calculations in order to match the measured plasma conditions. Including ionization also improves agreement with the measured spectra (Fig. 3). While Fig. 2 shows the need for non-Maxwellian distributions driven by inverse bremsstrahlung heating to reproduce the spectra, the electron density and temperature reveal the need to include an atomic physics model. Without ionization, it is not possible to match the density, which rises by $\sim$ 15% after the heating beam is turned off. During this time, the collisional ionization continues resulting in the rising density (Fig. 4). This process uses the kinetic energy of the free electrons to
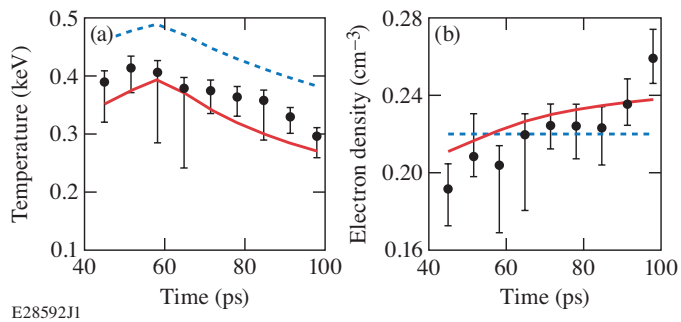
E28592J1

FIG. 4. The measured (a) temperature and (b) density (black circles) are compared to K2 simulation results. The black error bars represent a 95% confidence interval in the given parameter. The results of a K2 simulation without atomic kinetics (dashed blue curves) and the results of a K2 simulation with atomic physics (red curve) are shown.
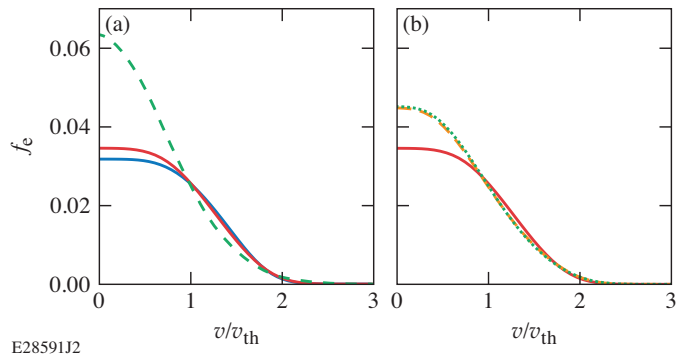

E28591J2

FIG. 5. (a) Electron distribution functions calculated by K2 when including (red curve) and not including (blue curve) the atomic physics model at the end of the heater beam (60 ps) compared with a Maxwellian electron distribution function (dashed green curve). (b) Electron distribution functions at 58 ps (red), 71 ps (orange) and 78 ps (green) calculated by K2 including the atomic physics model.

ionize the plasma further, thereby lowering the temperature. Without ionization, the simulations lack this energy loss mechanism and therefore overestimated the temperature by $\sim 15\%$ to 20%. In simulations without ionization, it is possible to alter the initial plasma conditions to achieve better agreement with the temperature (Fig. 3), but this results in distribution functions that generate spectra with poor agreement with the measured Thomson-scattering spectra. By coupling K2 with an atomic kinetics model, not only was it possible to account for the temperature and density evolution, the electron distribution functions were modified bringing the calculated Thomson-scattering spectra into better agreement with the measurements. The improved agreement can be seen (Fig. 3) in the slightly wider peak and lower central region of the model with ionization. Resulting in an improved minimum χ^2, which was 10% to 15% smaller than the model without atomic kinetics for each case. The improved spectral match in conjunction with the ability to reproduce the temperature and density evolution necessitate the inclusion of the atomic physic model.

To determine the impact of ionization on the electron distribution function, an atomic physics model was coupled to K2. An inelastic collsional operator, sometimes called a Boltzmann operator, was used to model the changes to the distribution due to all atomic processes. The time evolution of the atomic states were determined through a set of coupled rate equations. The collisional rates that enter the rate matrix were obtained from direct integration of the actual distribution. The atomic data (energy levels and cross sections) was constructed based on a screened hydrogenic model using the code Cretin [18]. While the model used for these simulations includes different types of collisional and radiative processes (both bound-bound and bound-free), collisional ionization was identified as the main atomic process affecting the distribution function [7]. The simulations were performed using the experimental laser conditions. Simulations per-

formed without the atomic physics model used a preionized plasma with an electron density of 2.2×10^{19} cm^{-3} (corresponding to an average ionization state of 9.1) and an electron temperature of 10 eV. When using the atomic physics model, ionization was self-consistently included and the simulations were initialized with a neutral density of 2.4×10^{18} cm^{-3}.

Figure 5(a) shows the relative contributions of inverse bremsstrahlung heating, thermal transport, and atomic physics on the electron distribution function. The main deviation from Maxwellian was due to inverse bremsstrahlung heating and results in a reduction of slow electrons and an increase in electrons with a velocity of $\sim 1.5 v_{th}$. Heat transport compounds with the effect of inverse bremsstrahlung heating by further increasing the number of bulk electrons. The electrons in the tail of the electron distribution function carry heat away from the Thomson-scattering volume while the slower electrons, that maintain charge neutrality, reinforce the bulk of the electron distribution function. Ionization suppresses the super-Gaussian shape by preferentially removing electrons from around $2 - 3 v_{th}$ and supplying electrons with little to no velocity.

Figure 5(b) shows how the distribution function evolves. The electron distribution at 58 ps, while the heater beam is on, has been driven to a non-Maxwellian shape. It rapidly (< 10 ps) evolves to a new super-Gaussian distribution, but is still non-Maxwellian. Once this new electron distribution has been realized, the evolution slows and only small changes to the distribution continue through the end of the measurement (100 ps).

In summary, ultrafast Thomson-scattering measurements of the electron plasma wave spectrum were used to determine the effects of laser heating and ionization on the electron distribution function. While the argon plasma was being heated, super-Gaussian electron distri-

bution functions were measured. After the heater beam was turned off, the electron density continued to rise and the electron temperature dropped as the free electrons continued to ionize the argon plasma. The non-Maxwellian electron distribution functions from Vlasov-Fokker-Planck simulations that included both laser heating and ionization were required to reproduce the measured Thomson-scattering spectra, temperature evolution, and density evolution simultaneously. Thereby demonstrating the interplay between the effects of inverse bremsstrahlung and atomic kinetics on the shape of the electron distribution function. These results reinforce the importance of using non-Maxwellian electron distribution functions in determining plasma conditions from Thomson-scattering measurements.

[1] A. B. Langdon, Phys. Rev. Lett. **44**, 575 (1980).
[2] J. P. Matte, M. Lamoureux, C. Moller, R. Y. Yin, J. Delettrez, J. Virmont, and T. W. Johnston, Plasma Phys. Control. Fusion **30**, 1665 (1988).
[3] E. Fourkal, V. Y. Bychenkov, W. Rozmus, R. Sydora, C. Kirkby, C. E. Capjack, S. H. Glenzer, and H. A. Baldis, Phys. Plasmas **8**, 550 (2001).
[4] R. J. Henchen, M. Sherlock, W. Rozmus, J. Katz, D. Cao, J. P. Palastro, and D. H. Froula, Physical Review Letters **121**, 125001 (2018).
[5] W. Rozmus, T. Chapman, A. Brantov, B. J. Winjum, R. L. Berger, S. Brunner, V. Y. Bychenkov, A. Tableman, M. Tzoufras, and S. Glenzer, Physics of Plasmas **23**, 012707 (2016).
[6] L. Yin, B. J. Albright, K. J. Bowers, W. Daughton, and H. A. Rose, Physical Review Letters **99**, 265004 (2007).
[7] H. P. Le, M. Sherlock, and H. A. Scott, Physical Review E **100**, 013202 (2019).
[8] H. G. Rinderknecht, P. A. Amendt, S. C. Wilks, and G. Collins, Plasma Physics and Controlled Fusion **60**, 064001 (2018).
[9] J. M. Liu, J. S. De Groot, J. P. Matte, T. W. Johnston, and R. P. Drake, Phys. Rev. Lett. **72**, 2717 (1994).
[10] S. H. Glenzer, W. E. Alley, K. G. Estabrook, J. S. De Groot, M. G. Haines, J. H. Hammer, J. P. Jadaud, B. J. MacGowan, J. D. Moody, W. Rozmus, L. J. Suter, T. L. Weiland, and E. A. Williams, Physics of Plasmas **6**, 2117 (1999).
[11] V. Bagnoud, I. A. Begishev, M. J. Guardalben, J. Puth, and J. D. Zuegel, Optics Letters **30**, 1843 (2005).
[12] A. M. Hansen, D. Haberberger, J. Katz, D. Mastrosimone, R. K. Follett, and D. H. Froula, Review of Scientific Instruments **89**, 10C103 (2018).
[13] J. Katz, R. Boni, R. Rivlis, C. Muir, and D. H. Froula, Review of Scientific Instruments **87**, 11E535 (2016).
[14] A. S. Davies, D. Haberberger, J. Katz, S. Bucht, J. P. Palastro, W. Rozmus, and D. H. Froula, Physical Review Letters **122**, 155001 (2019).
[15] A. L. Milder, S. T. Ivancic, J. P. Palastro, and D. H. Froula, Physics of Plasmas **26**, 022711 (2019).
[16] R. K. Follett, J. A. Delettrez, D. H. Edgell, R. J. Henchen, J. Katz, J. F. Myatt, and D. H. Froula, Review of Scientific Instruments **87**, 11E401 (2016).
[17] M. Sherlock, J. P. Brodrick, and C. P. Ridgers, Physics of Plasmas **24**, 082706 (2017).
[18] H. A. Scott and S. B. Hansen, High Energy Density Physics **6**, 39 (2010).